

MULTIRESOLUTION TENSOR DECOMPOSITION FOR MULTIPLE SPATIAL PASSING NETWORKS

BY SHAOBO HAN, AND DAVID B. DUNSON

Department of Statistical Science, Duke University

This article is motivated by soccer positional passing networks collected across multiple games. We refer to these data as *replicated spatial passing networks*—to accurately model such data it is necessary to take into account the spatial positions of the passer and receiver for each passing event. This spatial registration and replicates that occur across games represent key differences with usual social network data. As a key step before investigating how the passing dynamics influence team performance, we focus on developing methods for summarizing different team’s passing strategies. Our proposed approach relies on a novel multiresolution data representation framework and Poisson nonnegative block term decomposition model, which automatically produces coarse-to-fine low-rank network *motifs*. The proposed methods are applied to detailed passing record data collected from the 2014 FIFA World Cup.

1. Introduction. We are interested in studying the ball passing patterns of soccer teams. Passing is one of the key parts in soccer, possessing valuable information about different playing styles from across the world. As illustrated in Figure 1, one team’s spatial passing record E aggregated in a game consists of J number of ball passing-receiving events $\{e_j : j = 1, \dots, J\}$ on the soccer field. Each event e_j corresponds to a pass observed from origin node (x_j^o, y_j^o) to destination node (x_j^d, y_j^d) , both embedded in the soccer field—a two-dimensional rectangle space $\mathcal{F} \subset \mathbb{R}^2$. Passing data for all the 32 teams in 64 matches of the FIFA World Cup 2014 in Brazil are available.

With the recent development of optical tracking systems and video extraction software, team-based human activities in professional sports are now routinely monitored at high spatiotemporal resolution, which opens up new avenues for quantitative characterization of team strategies and performance enriched with spatiotemporal structures. Recent advances along these lines have been made in the context of professional basketball. [Miller et al. \(2014\)](#) provide a quantitative summary of shooting habits and efficiency of basketball players, based on spatial locations of shot attempts made by NBA players on the offensive half court. [Franks et al. \(2015\)](#) further identify the

Keywords and phrases: higher-order tensor, multivariate contingency table, multiresolution methods, nonnegative block term decomposition, replicated networks

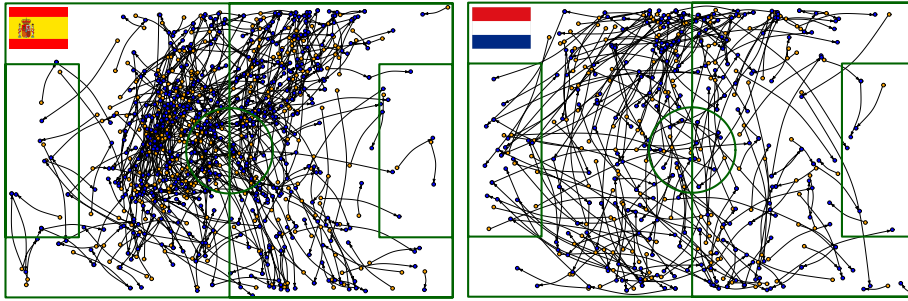


FIG 1. *Spatial passing networks in a 2014 FIFA world cup match (Spain 1-5 Netherlands). 540 completed passes recorded for Spain (left) and 276 completed passes recorded for the Netherlands (right). A pair of orange and blue nodes indicates the origin-destination of a pass. Team's direction of attack: from left to right.*

intent of defenders and quantify the effect they have on both shot frequency and efficiency from player and ball tracking data. [Cervone et al. \(2016\)](#) focus on modeling players' decision making tendencies in various situational, spatiotemporal circumstances and predicting expected number of points the offense will score on a particular possession.

While basketball is a high scoring game with very frequent shooting attempts and relatively simple passing dynamics, soccer is very low scoring and much of the game involves intricate passing configurations, which occasionally lead to shot attempts. Soccer is more a game of space invasion that is mainly undertaken through passes. It is interesting to identify interpretable summary *motifs* representing a small set of passes that teams often employ. However, the current literature lacks such methodology — typically focusing on simple summary statistics of team passing that ignore spatial information.

Traditionally, team's passing performance is summarized in one easy-to-calculate yet overly simplified statistic, e.g., the possession percentage as a measure of team dominance. Network graphs improve upon it by providing us a simple characteristic abstraction of team's passing behavior. For example, [Duch, Waitzman and Amaral \(2010\)](#), [Peña and Touchette \(2012\)](#) and [Cintia, Rinzivillo and Pappalardo \(2015\)](#) investigate player passing networks in which nodes are players and directed edges are passes and zone passing networks in which nodes are divided regions of the soccer field and edges are cumulative number of ball displacements between pairs of regions. These articles reduce network topological structure into simple metrics, such as node degree, betweenness and closeness centralities, clustering coefficients, etc., therefore mostly focusing on providing high-level overviews of topological

structures of a *single* passing network. Although these network descriptors offer valuable insights in evaluating different aspects of teamwork performance, statistical and generative modeling for the observed passing patterns of *multiple* teams (potentially under different conditions) would provide a more comprehensive understanding of the characteristics of team’s strategies, aiding the design, planning and selection of competitive soccer tactics at the team level.

There is a rich literature on statistical network models; see [Goldenberg et al. \(2010\)](#) and [Schmidt and Morup \(2013\)](#) for reviews. There has been an enormous emphasis in the literature on node community detection [[Holland, Laskey and Leinhardt \(1983\)](#), [Nowicki and Snijders \(2001\)](#), [Airoldi et al. \(2008\)](#)], especially for single, undirected, binary networks. In our motivating application of soccer passing analytics, partitioning links [[Ahn, Bagrow and Lehmann \(2010\)](#), [Ball, Karrer and Newman \(2011\)](#), [Zhou \(2015\)](#)] into latent passing combination groups is a more meaningful goal than clustering nodes into groups. Extensions of these methods to directed and weighted networks are straightforward, but the replicated aspect requires careful innovation. Besides flexibly capturing assortative and disassortative structures [[Hoff \(2008\)](#)] within each single network, it is important to exploit the co-occurrence information across multiple networks and extract archetypal motifs, which could serve as building blocks for network comparison and predictive modeling.

Team’s passing history is synthesized under the form of spatial networks [[Barthélemy \(2011\)](#)] where nodes and edges are embedded in a rectangle soccer field space (115 yards \times 74 yards with slight variations). This is another relevant characteristic of the soccer passing network. The X and Y co-ordinates of origin-destination locations of a pass possess important information about its type (e.g., short passes, long passes, flick-on, or pull back) and directions (e.g., backwards, sideways, or forwards). The soccer field is typically divided into several zones, either own half/opposition half, defensive/middle/final third, left/right/centre, or more elaborate Guardiola positional grids. There is no consensus upon the best approach to this division. Different division results in explaining the strategic and tactical peculiarities of the team play at different spatial resolutions. Besides the network topology, it is crucial to take the spatial structure inherent in these types of networks into account, and accommodate potential multi-resolution behaviors.

1.1. *Replicated spatial passing networks.* We focus on the passing data from the 2014 FIFA World Cup in Brazil. 32 national teams advanced to the

final tournament and a total of 64 matches were played. For each match, every completed pass is logged with X and Y coordinates for its point of origin and destination. Although most passes do not lead directly to goals, they do manifest the team playing style in collaboration, partly in response to the defenses being faced with shots on goal relatively rare. These dynamics potentially vary across teams and matches. Instead of analyzing single passing networks separately, we are focused on *replicated* passing networks, which can be considered as realizations from some distribution over the space of all possible passing networks. The concept of replicated networks was introduced in [Durante, Dunson and Vogelstein \(2017\)](#) motivated by neuroscience applications. To emphasize the replicated, spatial aspects, and the directional asymmetry of our special type of networks, we use the terminology *replicated spatial passing networks*.

As an initial attempt, we construct each of the 32 team’s spatial networks $\mathcal{G}_t = \{\mathcal{V}_t, \mathcal{E}_t\}$ by dividing up the field into a grid of tiles, $t = 1, \dots, 32$, with each tile in this grid representing a node and the weighted edge given by the total J_t number of passes going between the pair of nodes, aggregated from all the 3 to 7 matches that team played. Each network is naturally represented as a weighted adjacency matrix A_t of size $|\mathcal{V}_t| \times |\mathcal{V}_t|$, where $|\mathcal{V}_t|$ is the number of tiles. We evaluate the Bray-Curtis dissimilarity [[Bray and Curtis \(1957\)](#)] between teams based on vectorization of adjacency matrices. To ensure that the same physical sample size assumption of Bray-Curtis statistics was met, we scale the cumulative number of passes by the ratio between the mean participating time (384.875 minutes) and team’s actual total participating minutes in the whole tournament. Hence, the Bray-Curtis dissimilarity measure takes into account the higher rate of completed passes as part of the difference between teams.

As shown in [Figure 2](#), the Bray-Curtis dissimilarities between team passing networks are evaluated at three scales from coarse to fine. Under relatively coarse spatial resolution, substantial information on finer scales is discarded and team networks tend to behave more similarly to each other. On the contrary, finer spatial resolution is able to preserve high fidelity of the passing network but renders the sharing of statistical strength among multiple networks very difficult. Motivated by our replicated spatial passing network data and the pressing need for appropriately borrowing information across scales and replicates, we develop a Multiresolution Tensor (MrTensor) decomposition approach on a stack of multiresolution adjacency tensors, which can learn coherent coarse-to-fine subnetwork representations from fine-grained relational event data.

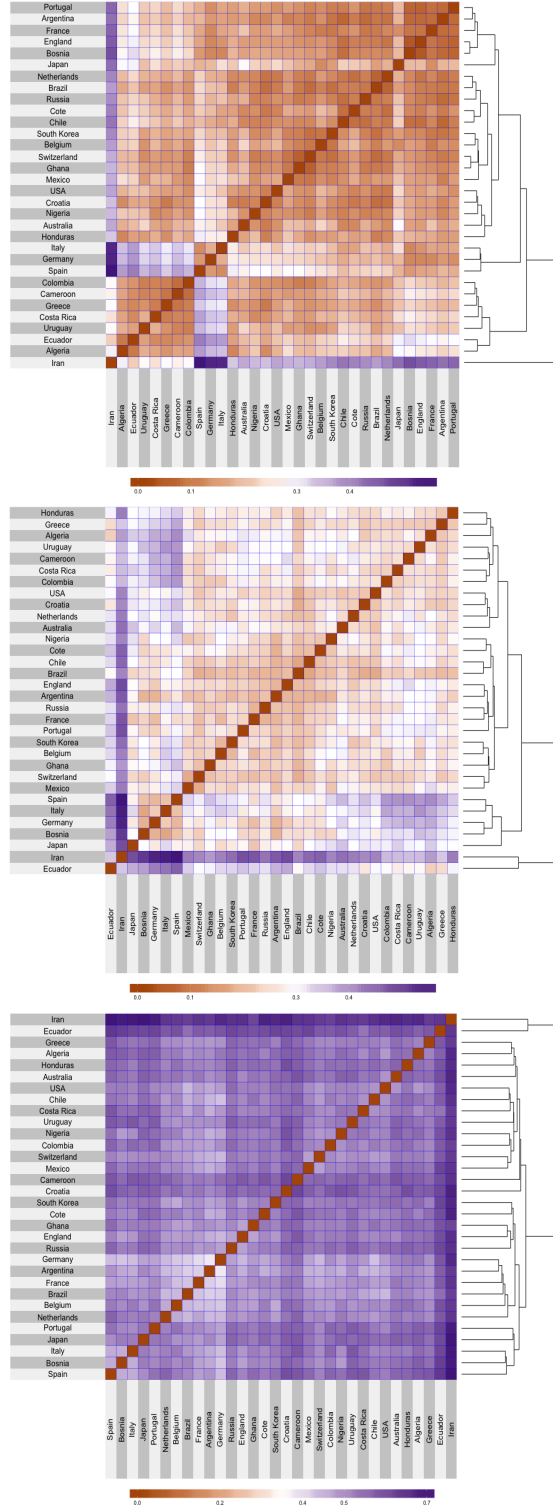


FIG 2. Bray-Curtis dissimilarity (bounded between 0 and 1) between each pair of the 32 teams in 2014 FIFA world cup. Each team's passing strategy is characterized by a weighted adjacency matrix of a directed graph, built based on the adjusted cumulative number of passes between different areas of the soccer field in all its games. We uniformly divide the field into 2×2 (top), 4×4 (middle) and 8×8 (bottom) areas, leading to 4×4 , 16×16 , 64×64 weighted adjacency matrices under three different spatial resolutions.

1.2. *Relevant literature.* There is an emerging literature on statistical modeling of replicated networks. Much of the literature deals with binary symmetric matrix representations of networks; see, for example, [Durante, Dunson and Vogelstein \(2017\)](#), [Durante et al. \(2017\)](#) and [Wang et al. \(2017\)](#). We instead consider the case in which fine-grained, directed and weighted spatial network data are available and the spatial locations of nodes play a vital role in data organization.

Passes from $(x_j^o, y_j^o) \in \mathcal{F}$ to $(x_j^d, y_j^d) \in \mathcal{F}$ can be viewed as dyadic events in product space $\mathcal{F} \times \mathcal{F} \subset \mathbb{R}^4$. These data can potentially be viewed as spatial point patterns, with appropriate continuous process models developed. Modeling point patterns as spatial point processes [[Møller and Waagepetersen \(2007\)](#); [Baddeley, Bárány and Schneider \(2007\)](#)] in continuous space is conceptually simple, but often computationally cumbersome due to intractable integrals. To simplify computation, we instead take a fine-grained discretization of the space based on a multiresolution tiling scheme and focus on the underlying structures driving the global variations across replications, while sacrificing the ability of modeling subtle local variations within each cell of the division. Related discretization procedures were employed by [Miller et al. \(2014\)](#) and [Franks et al. \(2015\)](#) in modeling of NBA shot data.

In this application as well as in many other applications (e.g., brain connectomes), networks are spatially embedded and nodes are non-exchangeable, which hinders the utility of exchangeable graph models [[Orbanz and Roy \(2015\)](#); [Caron and Fox \(2017\)](#)] developed based on Aldous-Hoover or Kallenberg representation theorems. Exploiting the spatial information, a recursive division of the soccer field can naturally induce nested hierarchies within a single network and correspondences of nodes across replicates, that allow us to perform joint multiscale analysis of passing patterns in multiple networks.

In Section 2 we describe a binary encoding scheme and our MrTensor framework. To flexibly characterize the generative mechanism of replicated networks and reduce dimensionality, we postulate passing networks as a weighted combination of low-rank network motifs and introduce a nonnegative tensor decomposition model for multiresolution adjacency tensors in Section 3. In Section 4, we exploit sparsity in the data and propose an efficient optimization algorithm based on block coordinate descent procedures with adaptation of model dimensions. Section 5 presents the results for our analysis of real data.

2. Multiresolution Tensor Representation.

2.1. *Tensorial data structure.* We divide the standardized rectangle soccer field uniformly into $L \times L$ tiles and represent a pass observed in replicate

n in tensor indices format $\mathbf{i} = (i_1, \dots, i_K, n)^T$, with $i_k \in \{0, \dots, L - 1\}$ having L levels, $n \in \{1, \dots, N\}$ having N levels, and $k = 1, \dots, K$. Comparing against the conventional adjacency matrices representation of network data, this multi-indices representation has the potential advantages of being more compact and informative; (i) it implicitly preserves the network connectivity information by storing only the link observed, (ii) it explicitly expresses the nodal attributes (e.g., tile coordinates), (iii) it is easily expandable to incorporate additional edge properties such as the type of the pass or replicated-level attributes such as the competition outcome. The whole indices list can be conveniently represented as a $K + 1$ dimensional contingency table \mathbf{X}_0 , or in other words, a $K + 1$ way count valued tensor, with $N \times L^K$ cells in total. The value in each cell denotes the number of occurrences. In our particular case, $K = 4$, and \mathbf{i} denotes a pass from origin tile (i_1, i_2) to destination tile (i_3, i_4) conducted by subject t . The stacked adjacency matrices representation of multiple networks can be conveniently induced via unfolding the 5-way tensor of size $N \times L^4$ into a 3-way tensor of size $N \times L^2 \times L^2$ where multi-indices $\mathbf{i}' = \{(i_1, i_2), (i_3, i_4), t\} = \{i^o, i^d, t\}$, $i^o = i_1 + (i_2 - 1)L$, $i^d = i_3 + (i_4 - 1)L$ are the indices for the origin tile and destination tile, respectively.

2.2. Binary encoding scheme. Passing endeavors can be viewed as hierarchical resource allocation on the field, assigned by teams in possession with the objectives of maneuvering through the defense and creating better chances to score. Teams' passing selections are arguably influenced heavily by different soccer philosophies of strategic planners at macroscopic spatial resolutions and perturbed by situational circumstances or observation noise at fine spatial resolutions. With this motivation, we model the spatial passing networks in a multiscale manner, with coarse-to-fine representations gradually informed by events on multiple spatial scales.

To access the multiscale occurrence information, we apply a recursive dyadic partitioning scheme uniformly on the soccer field rectangle \mathcal{F} along both the vertical and horizontal directions. So on each scale, a region is further split into four non-overlapping subregions of the same size. Letting $L = 2^S$, along each direction the spatial intervals i_k are treated as categorical variables taking values in $\{0, \dots, 2^S - 1\}$. This recursive dyadic partitioning procedure corresponds to a binary encoding scheme that converts a categorical variable i into an S bit binary code $\mathbf{b}_{1:S}(i)$, more precisely, $i = \sum_{s=1}^S b_s(i) \times 2^{S-s}$, $b_s(i) \in \{0, 1\}$. See Figure 3 for an illustrative example, the location of an event in cell $(3, 4)_{10}$ is reparameterized as $(011, 100)_2$. Accordingly, the event can be located on three increasingly finer and finer

scales via binary codes (0,1)-red region, (01,10)-green region, (011,100)-purple region, respectively.

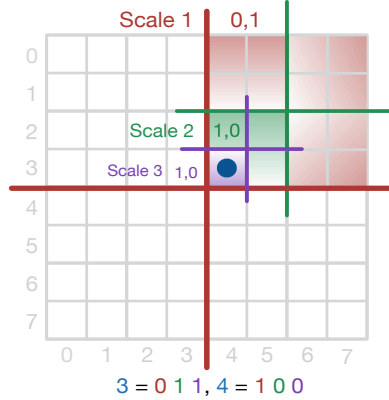


FIG 3. Coarse-to-fine dyadic partitioning and binary encoding. The 3-bits binary encoding on indices pairs corresponds to applying recursive dyadic partitioning three times on both sides of the rectangle.

We apply this binary encoding scheme to all the first $K = 4$ physical modes in the original indices $\bar{\mathbf{i}} = \{i_1, i_2, i_3, i_4\}$, which specify the spatial locations of passes. This reparameterization converts the multivariate categorical variables into higher dimensional multivariate binary variables, thus create S auxiliary modes for each of the 4 physical modes in the original tensor \mathfrak{X}_0 . To present it more concisely, in Table 1, we organize the resulting binary codes for spatial indices $\bar{\mathbf{i}}$ into a $K \times S$ table $\mathbf{B}(\bar{\mathbf{i}}) := \{b_s(i_k)\}_{k=1:K, s=1:S} = b_{s,k}$, where the column vector $\mathbf{b}_{s,1:K}$ stores information on scale s across all the physical location modes ($s = 1, \dots, S$ with 1 representing the coarsest scale, and S representing the finest scale), and the row vector $\mathbf{b}_{1:S,k}$ keeps the information in the k th physical mode across all scales. Accordingly, the augmented indices list with subject mode can be lodged in a $KS+1$ dimensional contingency table $\tilde{\mathfrak{X}}$, having the same number of cells as \mathfrak{X}_0 .

TABLE 1
The resulting binary codes reexpressed as an indices matrix $\mathbf{B}(\bar{\mathbf{i}})$

		Virtual scale modes			
		$s = 1$	$s = 2$	\dots	$s = S$
Physical location modes	$k = 1$	$b_1(i_1)$	$b_2(i_1)$	\dots	$b_S(i_1)$
	$k = 2$	$b_1(i_2)$	$b_2(i_2)$	\dots	$b_S(i_2)$
	\vdots	\vdots	\vdots	\ddots	\vdots
	$k = K$	$b_1(i_K)$	$b_2(i_K)$	\dots	$b_S(i_K)$

This binary reparameterization of multivariate categorical variables al-

lows us to characterize multiscale occurrence of an event. Referring to Figure 4, we denote a pass occurs from tile A to tile B in the multi-indices format $\vec{i} = (1, 6, 4, 3)$. It is then encoded on $S = 3$ scales as $\mathbf{B}(\vec{i}) := [\mathbf{b}_1(\vec{i}_{1:4}), \mathbf{b}_2(\vec{i}_{1:4}), \mathbf{b}_3(\vec{i}_{1:4})]$ with $\mathbf{b}_{1,1:4} = \mathbf{b}_1(\vec{i}_{1:4}) = (0, 1, 1, 0)$, $\mathbf{b}_{2,1:4} = \mathbf{b}_2(\vec{i}_{1:4}) = (0, 1, 0, 1)$, and $\mathbf{b}_{3,1:4} = \mathbf{b}_3(\vec{i}_{1:4}) = (1, 0, 0, 1)$. The binary codes of increasing lengths pertain to information observed on increasingly finer scales: (i) a pass from red rectangle zone $(0, 1)$ to zone $(1, 0)$ on scale 1, (ii) a pass from green rectangle zone $(00, 11)$ to zone $(10, 01)$ on scale 2, and (iii) a pass from purple rectangle zone $(001, 110)$ to zone $(100, 011)$ on scale 3.

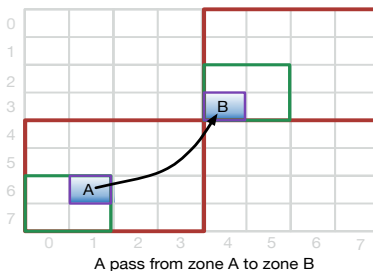


FIG 4. An event observed on three scales (red/green/purple rectangle pairs)

Tree-based multiresolution methods are prevalent in signal and image processing [Willsky (2002)]. The binary reparameterization implicitly induces a multiresolution (MR) tree of depth S , in which each internal node has 2^K children. For each network, the count of the number of occurrences at the 2^{KS} leaves of the tree can be organized in a tensor with KS modes. Consequently, the counts at coarser scales on the MR tree obtained by summing “children” counts can be conveniently found by marginalizing out the tensor modes relevant with finer scales.

The probability of an event $E_{(1:S')} := E_{(1)} \times \dots \times E_{(S')}$ viewed on scale S' ($S' = 2, \dots, S$) can be represented as

$$\Pr(E_{(1)}, \dots, E_{(S')}) = \Pr(E_{(1)}) \times \prod_{s=2}^{S'} \Pr(E_{(s)} | E_{(1)}, \dots, E_{(s-1)}),$$

where $\Pr(E_{(1)})$ can be interpreted as root proportion on the coarsest scale, $\Pr(E_{(s)} | E_{(1)}, \dots, E_{(s-1)})$ can be interpreted as coarse-to-fine splitting proportions moving from scales $s - 1$ to s , $s = 2, \dots, S$.

Related to our work, Kolaczyk (1999) proposes a recursive dyadic partition tree based Bayesian multiscale model for (discretized) intensity estimation in univariate inhomogeneous Poisson processes. However, the number of

parameters grows much faster with scales in multivariate cases. With suitable multilinear structures accompanied with specific mode-wise constraints, our proposed multiresolution tensorial representation can be a more compact and parsimonious alternative to the tree-structured parameterization.

2.3. Multiresolution adjacency tensor. Treating each network in an unstructured form corresponds to the traditional operation of *vectorization*, which flattens the $K + 1$ way tensor \mathfrak{X}_0 into a $L^K \times N$ matrix, such that each subject network is represented by a $L^K \times 1$ column vector. Unfortunately, this operation throws away the multiscale topological structure and creates huge dimensionality relative to the number of subjects. As a result, the associated matrix factorizations are likely to be poorly estimated. On the contrary, the above binary reparameterization scheme leads to an operation of *tensorization*, which folds the lower-dimensional tensor (matrix or vector) into a higher-dimensional one.

Interested in the multiscale topological structure of passing networks, we propose the *multiresolution adjacency tensor* representation of multiple networks in which passing networks on scale S are represented in the tensor indices format $\{i_1^o, i_1^d, \dots, i_S^o, i_S^d, n\}$. With $S = 3$, we transform the $KS + 1 = 13$ way tensor $\tilde{\mathfrak{X}}$ into a 7 way tensor \mathfrak{X} of the size $4 \times 4 \times 4 \times 4 \times 4 \times 4 \times N$, by mapping the tensor indices as follows,

$$\left\{ \underbrace{(\tilde{b}_{1,1}, \tilde{b}_{1,2})}_{i_1^o}, \underbrace{(\tilde{b}_{1,3}, \tilde{b}_{1,4})}_{i_1^d}, \underbrace{(\tilde{b}_{2,1}, \tilde{b}_{2,2})}_{i_2^o}, \underbrace{(\tilde{b}_{2,3}, \tilde{b}_{2,4})}_{i_2^d}, \underbrace{(\tilde{b}_{3,1}, \tilde{b}_{3,2})}_{i_3^o}, \underbrace{(\tilde{b}_{3,3}, \tilde{b}_{3,4})}_{i_3^d}, n \right\},$$

where $i_s^o = \tilde{b}_{s,1} + 2(\tilde{b}_{s,2} - 1)$, $i_s^d = \tilde{b}_{s,3} + 2(\tilde{b}_{s,4} - 1)$, $\tilde{b}_{s,k} \in \{1, 2\}$, $i_s^o, i_s^d \in \{1, 2, 3, 4\}$, $k = 1, \dots, 4$, $s = 1, 2, 3$. The number of cells in \mathfrak{X} does not change during this transformation. For subject t , the $4^s \times 4^s$ weighted adjacency matrix on scale s can be recovered via *matricization* [Kolda and Bader (2009)] of the tensor slice. Operating on the multi-indices, tensor element $\{i_1^o, i_1^d, \dots, i_s^o, i_s^d, n\}$ maps to matrix element (v_s^o, v_s^d, n) , where

$$\begin{aligned} v_1^o &= i_1^o, & v_1^d &= i_1^d, & v_1^o, v_1^d &\in \{1, \dots, 4\}, \\ v_2^o &= i_2^o + 4(v_1^o - 1), & v_2^d &= i_2^d + 4(v_1^d - 1), & v_2^o, v_2^d &\in \{1, \dots, 16\}, \\ v_3^o &= i_3^o + 4(v_2^o - 1), & v_3^d &= i_3^d + 4(v_2^d - 1), & v_3^o, v_3^d &\in \{1, \dots, 64\}. \end{aligned}$$

The elements in these adjacency matrices denote the edge weights. The edge weight on a coarser scale is an aggregation of its “children” edge weights on finer scales.

The idea of tensorization is proposed by Oseledets (2010) and Khoromskij (2011) in the context of quantized tensor networks. Accompanied by various

tensor factorization techniques, the effectiveness of tensorization in reducing storage burden and accelerating large-scale computations has been demonstrated with a wide range of successful applications to data compression, computational quantum chemistry and finite element method. Built upon similar ideas of tensorization—“blessing of dimensionality” [Cichocki et al. (2015)], we focus on combating the challenge of high dimensionality and low sample size, and discovering latent structures with natural interpretations by taking advantage of the intrinsic multiway and multiscale structure in the data.

3. Poisson Block Term Decomposition Model. The MrTensor data representation framework introduced in Section 2 is compatible with many off-the-shelf tensor decomposition routines and opens the door to other customized probabilistic models. In our applications of interest, data sparsity arises as the primary technical challenge in modeling. For moderate to high-resolution, we end up with massively more cells than the number of observed passes (is $\tilde{J} = \sum_{n=1}^N J_n = 44,125$), so the overwhelming majority of the cell counts will be zero. Choosing $S = 3$, the number of cells in \mathfrak{X} is $4 \times 4 \times 4 \times 4 \times 4 \times 4 \times 128 = 524,288$, with 32,143 of them non-zero (sparsity level: 93.87%). This sparsity issue is very common in analyzing multivariate categorical variables [Zhou et al. (2015)]. To combat this challenge, it is important to take advantage of a multilinear structure to build up the high dimensional tensor object with low-dimensional, and parsimonious matrices. On the other hand, the sparsity in the adjacency tensor also offers us an opportunity to save memory usage and running time, especially in applications with large-scale networks.

3.1. *Modeling weighted adjacency tensors.* Denote the i th element of the count valued tensor \mathfrak{X} as $x_{\mathbf{i}}$, where \mathbf{i} is a length 7 indices vector. (i_1, i_2) , (i_3, i_4) , (i_5, i_6) correspond to three scales (coarse-to-fine) and (i_1, i_3, i_5) and (i_2, i_4, i_6) correspond to the origin tile and destination tile, respectively, and i_7 is the index for replicates. To represent the intensity of each weighted passing network as a superposition of H archetypal network motifs $\{\mathfrak{D}_h\}_{h=1:H}$, we propose the following Poisson factorial model for the adjacency tensor,

$$x_{\mathbf{i}',n} \stackrel{ind.}{\sim} \text{Poisson}(\lambda_{\mathbf{i}',n}), \quad \lambda_{\mathbf{i}',n} = \sum_{h=1}^H d_{\mathbf{i}',h} v_{h,n},$$

where $\mathbf{i} = (\mathbf{i}', n)$, $\mathbf{i}' = (i_1, \dots, i_6)$, $t = 1, \dots, 128$. \mathfrak{D}_h is a $4 \times 4 \times 4 \times 4 \times 4 \times 4$ probability tensor of the same size as \mathfrak{X}_n , $v_{h,n} \geq 0$ determines the prevalence

of motif h in passing network n , $h = 1, \dots, H$, $n = 1, \dots, 128$. Equivalently, this model can be expressed as,

$$\mathbf{X}_n = \sum_{h=1}^H \mathbf{X}_{h,n}, \quad \mathbf{X}_{h,n} \sim \text{Multinomial}(J_{h,n}; \mathcal{D}_h), \quad J_{h,n} \sim \text{Poisson}(v_{h,n}),$$

that is, the adjacency tensor \mathbf{X}_n of passing network n can be randomly partitioned into H subnetworks represented by $\mathbf{X}_{h,n}$. Each subnetwork is constructed by distributing Poisson number of passes $J_{h,n}$ according to the probability tensor \mathcal{D}_h shared by all replicates. To ensure the model has greater flexibility in capturing structures and patterns inherent in the data, we set the number of motifs H to be large ($H \gg \max(I, N)$) such that the set of network motifs which represent the passing networks are over-complete [Lewicki and Sejnowski (2000)]. The degeneracy introduced by over-completeness can be resolved by incorporating additional constraints of sparsity.

3.2. Multiscale low-rank network motifs. In order to control the complexity in \mathcal{D}_h , one simple assumption is to constrain the probability tensor \mathcal{D}_h to be rank-one, i.e., $\mathcal{D}_h = \phi_h^{(1)} \circ \phi_h^{(2)} \circ \phi_h^{(3)} \circ \phi_h^{(4)} \circ \phi_h^{(5)} \circ \phi_h^{(6)}$, where \circ denotes the outer product, $\phi_h^{(p)}$ are probability vectors, $\phi_{i_p,h}^{(p)} \geq 0$, $\sum_{i_p=1}^I \phi_{i_p,h}^{(p)} = 1$, $p = 1, \dots, 6$, $I = 4$. This yields a nonnegative Poisson CANDECOMP/PARAFAC decomposition (Poisson CPD) model [Chi and Kolda (2012)],

$$\mathbf{X}_n \sim \text{Pois}(\mathbf{\Lambda}_n), \quad \mathbf{\Lambda}_n = \llbracket \mathbf{v}_n; \mathbf{\Phi}^{(1)}, \mathbf{\Phi}^{(2)}, \mathbf{\Phi}^{(3)}, \mathbf{\Phi}^{(4)}, \mathbf{\Phi}^{(5)}, \mathbf{\Phi}^{(6)} \rrbracket,$$

jointly applied on multiple adjacency tensors with shared factor matrices $\{\mathbf{\Phi}^{(p)}\}_{p=1:6}$. Here $\mathbf{\Lambda}_n = \llbracket \mathbf{v}_n; \mathbf{\Phi}^{(1)}, \dots, \mathbf{\Phi}^{(6)} \rrbracket$ is a shorthand notation for $\mathbf{\Lambda}_n = \sum_{h=1}^H v_{h,n} \phi_h^{(1)} \circ \dots \circ \phi_h^{(6)}$. However, the rank-one assumption on \mathcal{D}_h could be too restrictive in representing passing network motifs. Figure 5 shows several example motifs that are commonly seen passing combinations in soccer but are clearly not rank-one.

We relax this constraint by allowing \mathcal{D}_h to be low rank with the canonical polyadic decomposition structure,

$$\mathcal{D}_h = \sum_{r_h=1}^{R_h} \omega_{r_h,h} \phi_{r_h,h}^{(1)} \circ \phi_{r_h,h}^{(2)} \circ \phi_{r_h,h}^{(3)} \circ \phi_{r_h,h}^{(4)} \circ \phi_{r_h,h}^{(5)} \circ \phi_{r_h,h}^{(6)}.$$

Both ω_h and $\phi_{r_h,h}^{(p)}$ are constrained to be probability vectors. Each \mathcal{D}_h is a convex combination of rank-one components being consonant with the

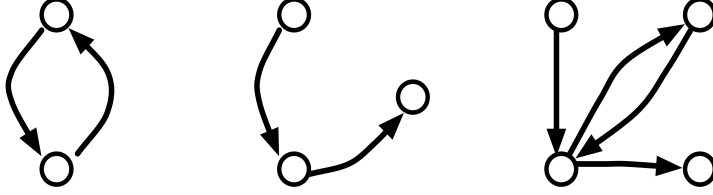


FIG 5. Three example low rank passing network motifs involving 2–4 nodes

multiresolution network topological structures. To see this, denoting the two coarser representations of \mathcal{D}_h on scale 1 and 2 as $\mathcal{D}_h^{(1)}$ and $\mathcal{D}_h^{(2)}$, we have

$$\mathcal{D}_h^{(1)} = \sum_{r_h=1}^{R_h} \omega_{r_h,h} \phi_{r_h,h}^{(1)} \circ \phi_{r_h,h}^{(2)}, \quad \mathcal{D}_h^{(2)} = \sum_{r_h=1}^{R_h} \omega_{r_h,h} \phi_{r_h,h}^{(1)} \circ \phi_{r_h,h}^{(2)} \circ \phi_{r_h,h}^{(3)} \circ \phi_{r_h,h}^{(4)},$$

so the R_h components are consistent across scales, $\{\phi_{r_h,h}^{(1)} \circ \phi_{r_h,h}^{(2)}\}$, $\{\phi_{r_h,h}^{(3)} \circ \phi_{r_h,h}^{(4)}\}$, and $\{\phi_{r_h,h}^{(5)} \circ \phi_{r_h,h}^{(6)}\}$ gradually adding more and more details to the representations on coarser scale through outer multiplication. This ensures our model finds coherent coarse-to-fine representations of low-rank motifs, which can serve as basic building blocks for secondary inference tasks such as team comparison and outcome prediction. Meanwhile, $\{\Phi_h^{(1)} \odot \Phi_h^{(3)} \odot \Phi_h^{(5)}\}$, $\{\Phi_h^{(2)} \odot \Phi_h^{(4)} \odot \Phi_h^{(6)}\}$ are the feature matrices for the sender nodes and receiver nodes in each partitioned network h on scale 3, where \odot denotes the Khatri-Rao product.

In tensor notation, this model can be summarized as,

$$\begin{aligned} \mathbf{X}_n &\sim \text{Pois}(\mathbf{\Lambda}_n), \quad \mathbf{\Lambda}_n = \sum_{h=1}^H \mathcal{D}_h v_{h,n}, \\ (3.1) \quad \mathcal{D}_h &= \llbracket \omega_h; \Phi_h^{(1)}, \Phi_h^{(2)}, \Phi_h^{(3)}, \Phi_h^{(4)}, \Phi_h^{(5)}, \Phi_h^{(6)} \rrbracket, \quad n = 1, \dots, N. \end{aligned}$$

All the parameters in equation (3.1) are constrained to be non-negative. We term the model as *Poisson nonnegative CP-Block Term Decompositions* (Poisson CP-BTD). The block term decomposition (BTD) [De Lathauwer (2008); De Lathauwer and Nion (2008)] refers to the decomposition of the higher-order tensor $\mathbf{\Lambda} \in \mathbb{R}^{4 \times 4 \times 4 \times 4 \times 4 \times 4 \times H}$ into a sum of rank $(R_h, R_h, R_h, R_h, R_h, R_h, 1)$ block terms,

$$\mathbf{\Lambda} = \sum_{h=1}^H \mathbf{\Lambda}_h = \sum_{h=1}^H \left(\text{diag}(\omega_h) \times_1 \Phi_h^{(1)} \times_2 \Phi_h^{(2)} \dots \times_6 \Phi_h^{(6)} \right) \circ v_h,$$

where \times_p denotes the mode- p tensor-matrix product and $\text{diag}(\boldsymbol{\omega}_h)$ denotes a $R_h \times R_h \times R_h \times R_h \times R_h \times R_h$ diagonal tensor. The diagonal entry $\omega_{r_h, h}$ determines the excitation of template $\phi_{r_h, h}^{(1)} \circ \dots \circ \phi_{r_h, h}^{(6)}$ in motif h . Our model can be viewed as a probabilistic extension of BTM in taking account of higher-order sparse count tensors. The nonnegative constraints allow for non-subtractive (part-based) representations of the network with natural interpretations [Lee and Seung (1999); Shashua and Hazan (2005)]. The notion of linear rank is therefore generalized to nonnegative rank [Cohen and Rothblum (1993)], so R_h can be larger than the original data dimension.

4. Block Coordinate Descent Algorithm. In Section 3 we proposed a Poisson CP-BTD model for the multiresolution adjacency matrices. The dependency structure of the underlying intensity parameter is captured by the CP-BTD model and the random variations of the individual count, is described by the Poisson distribution. Maximizing the Poisson log-likelihood is equivalent to minimizing the (generalized) Kullback-Leibler (KL) divergence up to an additive constant,

$$(4.1) \quad f(\boldsymbol{\Lambda}) = \sum_{\mathbf{i}} \lambda_{\mathbf{i}} - \sum_{\mathbf{i}: x_{\mathbf{i}} \neq 0} x_{\mathbf{i}} \log \lambda_{\mathbf{i}}, \quad \mathbf{i} = (i_1, \dots, i_P, n),$$

subject to the multilinear constraint on the underlying intensity parameters,

$$\lambda_{\mathbf{i}} = \sum_{h=1}^H v_{h, n} \sum_{r_h=1}^{R_h} \omega_{r_h, h} \prod_{p=1}^P \phi_{i_p, r_h, h}^{(p)}, \quad v_{h, n} \geq 0.$$

In order to remove scaling ambiguities, we impose both $\boldsymbol{\omega}_h$ and $\phi_h^{(p)}$ to be probability vectors, $\phi_{i_p, h}^{(p)} \geq 0$, $\sum_{i_p=1}^I \phi_{i_p, h}^{(p)} = 1$, $p = 1, \dots, P$, and $\omega_{r_h, h} \geq 0$, $\sum_{r_h=1}^{R_h} \omega_{r_h, h} = 1$, $h = 1, \dots, H$. The maximum likelihood solution for this model can be found by an expectation maximization (EM) algorithm, detailed in Appendix A. This algorithm has high consumption of memory as it requires storage of a $J \times (\sum_{h=1}^H R_h)$ intermediate matrix in the E-step of every iteration, where J is the number of nonzero cells in \mathcal{X} . Alternatively, we develop a block nonlinear Gauss-Seidel (GS) algorithm [Grippo and Scianrone (2000); Kim, He and Park (2014); Hansen, Plantenga and Kolda (2015)] for the Poisson CP-BTD model. In parallel with the alternating least square procedures in the BTM model which minimizes the Frobenius norm [De Lathauwer and Nion (2008)], the KL divergence minimization problem in Poisson BTM boils down to alternating Poisson regression (APR) [Chi and Kolda (2012)] steps. The algorithm is convergent with lower per-iteration cost and much greater memory efficiency.

4.1. *Nonlinear Gauss-Seidel method.* Our optimization problem is defined as

$$\begin{aligned}
 \min f(\mathbf{\Lambda}) &= \sum_{\mathbf{i}} \lambda_{\mathbf{i}} - \sum_{\mathbf{i}:x_{\mathbf{i}} \neq 0} x_{\mathbf{i}} \log \lambda_{\mathbf{i}}, \quad \text{s.t.} \quad \mathbf{\Lambda} = \sum_{h=1}^H \mathcal{D}_h \circ \mathbf{v}_h, \\
 \mathcal{D}_h &= \llbracket \boldsymbol{\omega}_h; \boldsymbol{\Phi}_h^{(1)}, \dots, \boldsymbol{\Phi}_h^{(P)} \rrbracket \in \mathcal{O}, \\
 \mathcal{O} &= \mathcal{O}_{\mathbf{Y}} \times \mathcal{O}_{\boldsymbol{\omega}_1} \times \dots \times \mathcal{O}_{\boldsymbol{\omega}_H} \times \mathcal{O}_{\boldsymbol{\Phi}^{(1)}} \times \dots \times \mathcal{O}_{\boldsymbol{\Phi}^{(P)}},
 \end{aligned}
 \tag{4.2}$$

where

$$\begin{aligned}
 \mathcal{O}_{\mathbf{Y}} &= [0, \infty)^{H \times N}, \\
 \mathcal{O}_{\boldsymbol{\omega}_h} &= \left\{ \boldsymbol{\omega}_h \in [0, 1]^{R_h \times 1} \mid \|\boldsymbol{\omega}_h\|_1 = 1 \right\}, \quad h = 1, \dots, H, \\
 \mathcal{O}_{\boldsymbol{\Phi}^{(p)}} &= \left\{ \boldsymbol{\Phi}^{(p)} \in [0, 1]^{I \times \sum_h R_h} \mid \|\boldsymbol{\phi}_{r_h, h}^{(p)}\|_1 = 1, \quad \forall (r_h, h) \right\}, \quad p = 1, \dots, P.
 \end{aligned}$$

We solve problem (4.2) via an alternating approach between updating the factor score matrix \mathbf{Y} and the mode-wise factor loading matrices $\{\boldsymbol{\Phi}^{(p)}\}_{p=1:P}$ composing the network motifs $\{\mathcal{D}_h\}_{h=1:H}$.

4.1.1. *Updating the factor score matrix.* We define $\boldsymbol{\Omega}$ to be an $R \times H$ matrix composed of the direct sum of $R_h \times 1$ column vectors $\boldsymbol{\omega}_h$. Specifically, $\boldsymbol{\Omega} = \bigoplus_{h=1}^R \boldsymbol{\omega}_h$, where \bigoplus is the direct sum, $R = \sum_{h=1}^H R_h$. The $(\prod_{p=1}^P I) \times H$ matrix representation of the network motif \mathcal{D} can be written as

$$\mathcal{D} = (\boldsymbol{\Phi}^{(P)} \odot \boldsymbol{\Phi}^{(P-1)} \odot \dots \odot \boldsymbol{\Phi}^{(1)}) \boldsymbol{\Omega},
 \tag{4.3}$$

with each row \mathbf{d}_h a probability vector which corresponds to a motif. The matricization of the $(P+1)$ -way tensor \mathcal{X} along its last mode results in a $(\prod_{p=1}^P I) \times N$ two-dimensional matrix \mathbf{X} . The optimization problem can be written as

$$\min_{\mathbf{Y} \geq 0} f(\mathbf{\Lambda}) \equiv \mathbf{e}^T [\mathcal{D} \mathbf{Y} - \mathbf{X} \circledast \log(\mathcal{D} \mathbf{Y})] \mathbf{e},$$

where \mathbf{e} is the vector of all ones, and \circledast is the Hadamard product between matrices. We further reduce memory usage and accelerate computation. First, note that most of the elements in matrix \mathbf{X} are zero, storing it as a sparse matrix in the indices format only requires $J(P+2)$ memory, with J the number of nonzero elements. Second, given \mathcal{D} , the objective function $f(\mathbf{\Lambda})$ is separable with respect to the columns of \mathbf{Y} , i.e., $f(\mathbf{\Lambda}) = \sum_{n=1}^N f_n(\mathbf{v}_n)$;

therefore, the N columns of \mathbf{Y} can be updated simultaneously. Third, denoting the subsets of indices $\mathbf{i}_n := \{\mathbf{i} : i_7 = n \text{ and } x_{\mathbf{i}} \neq 0\}$, $\bar{\mathbf{i}}_n := (i_{n,1}, \dots, i_{n,P})$ and $\mathbf{x}_n = \mathbf{X}[:, n]$, we have

$$(4.4) \quad \begin{aligned} f_n(\mathbf{v}_n) &= \mathbf{e}^T \mathbf{D} \mathbf{v}_n - \mathbf{x}_n^T \log(\mathbf{D} \mathbf{v}_n) \\ &= \sum_{h=1}^H v_{h,n} - \sum_{\mathbf{i}_n} \left[x_{\mathbf{i}_n} \log \left(\sum_{h=1}^H d_{\bar{\mathbf{i}}_n, h} v_{h,n} \right) \right]. \end{aligned}$$

In the first RHS term of the equation (4.4), we have $\mathbf{e}^T \mathbf{D} \mathbf{v}_n = \sum_{h=1}^H v_{h,n}$ due to the simplex constraint on the rows of \mathbf{D} . Therefore, we only need to compute and store a $J_n \times H$ submatrix of \mathbf{D} in which the J_n columns correspond to nonzero elements in the vector \mathbf{x}_n , that is,

$$(4.5) \quad \mathbf{D}^{[n]} = \left(\Phi^{(1)}[\mathbf{i}_{1,n}, :] \circledast \dots \circledast \Phi^{(P)}[\mathbf{i}_{P,n}, :] \right) \Omega.$$

The computations of equation (4.5) based on the Hadamond product of matrices are much cheaper than those of equation (4.3) based on the Khatri-Rao product. Minimizing $f_n(\mathbf{v}_n)$ can be viewed as finding the maximum likelihood solution of a Poisson linear regression problem with identity link, $\mathbf{D}^{[n]}$ is a $J_n \times H$ matrix, \mathbf{x}_n is a $J_n \times 1$ count-valued vector, and \mathbf{v}_n is the $H \times 1$ nonnegative regression coefficients. This problem is convex and the solver to this problem is introduced later in Section 4.2.

4.1.2. Updating the mode-wise factor loading matrices. Similarly, we unfold the $(P+1)$ -way tensor \mathcal{X} along its p -th mode, which results in a $(N \prod_{q \in \{1:P\} \setminus p} I_q) \times R$ two-dimensional matrix $\mathbf{X}^{(p)}$, $R = \sum_{h=1}^H R_h$. Letting the $R \times N$ matrix $\mathbf{S} = \Omega \mathbf{Y}$ with row sum $\boldsymbol{\tau} = \mathbf{S} \mathbf{e}$, for convenience of computation later, we set $\mathbf{T} = \text{diag}(\boldsymbol{\tau})$, $\Psi = \mathbf{T}^{-1} \mathbf{S}^T$ such that every column of Ψ is a probability vector. Again the corresponding $(N \prod_{q \in \{1:P\} \setminus p} I_q) \times R$ covariate matrix can be written as $\mathbf{B}^{(p)} = (\odot_{q \in \{1:P\} \setminus p} \Phi^{(q)}) \odot \Psi$ using Khatri-Rao product, the optimization objective function is

$$(4.6) \quad \min_{\Phi^{(p)}, \mathbf{T}} f(\Lambda) \equiv \mathbf{e}^T [\mathbf{B}^{(p)} \mathbf{T} \Phi^{(p)T} - \mathbf{X}^{(p)} \circledast \log(\mathbf{B}^{(p)} \mathbf{T} \Phi^{(p)T})] \mathbf{e},$$

such that

$$\Phi^{(p)} \in [0, 1]^{I \times \sum_h R_h}, \quad \left\| \phi_{r_h, h}^{(p)} \right\|_1 = 1, \quad \tau_{r_h, h} \geq 0, \quad \forall (r_h, h).$$

However, the feasible set of the optimization problem in equation (4.6) is no longer convex, due to the ℓ_1 norm equality constraint. Following Hansen,

Plantenga and Kolda (2015), we set $\mathbf{A}^{(p)} = \mathbf{\Phi}^{(p)}\mathbf{T}$, and rewrite the objective function in equation (4.6) as

$$\min_{\mathbf{A}^{(p)} \geq 0} f(\mathbf{\Lambda}) \equiv \mathbf{e}^T [\mathbf{B}^{(p)} \mathbf{A}^{(p)T} - \mathbf{X}^{(p)} \circledast \log(\mathbf{B}^{(p)} \mathbf{A}^{(p)T})] \mathbf{e},$$

which is convex with respect to $\mathbf{A}^{(p)}$. After finding $\mathbf{A}^{(p)}$, we set $\boldsymbol{\rho} = \mathbf{A}^{(p)}\mathbf{e}$ and $\mathbf{\Phi}^{(p)} = \mathbf{A}^{(p)}[\text{diag}(\boldsymbol{\rho})]^{-1}$ to ensure the simplex constraints on the columns of $\mathbf{\Phi}^{(p)}$ are satisfied. In addition, we let $\omega_{r_h, h} = \rho_{r_h, h} / \sum_{r_h=1}^{R_h} \rho_{r_h, h}$. This rescaling operation is also adopted by Chi and Kolda (2012) in their CP-APR algorithm.

Second, given $\mathbf{B}^{(p)}$, the objective function $f(\mathbf{\Lambda})$ is also separable with respect to the rows of $\mathbf{A}^{(p)}$. Letting $i_p = m$, denoting the subsets of indices $\mathbf{i}_m^{(p)} := \{\mathbf{i} : \mathbf{i}^{(p)} = m \text{ and } x_i \neq 0\}$, $\bar{\mathbf{i}}_m^{(p)} := (\mathbf{i}_m^{(p)}, \{1:P\} \setminus p, n_m^{(p)})$ and $\mathbf{x}_m^{(p)} = \mathbf{X}^{(p)}[:, m]$, $m \in \{1, \dots, I\}$, we have

$$\begin{aligned} f_m(\mathbf{a}_m^{(p)}) &= \mathbf{e}^T \mathbf{B}^{(p)} \mathbf{a}_m^{(p)} - \mathbf{x}_m^{(p)T} \log(\mathbf{B}^{(p)} \mathbf{a}_m^{(p)}) \\ (4.7) \quad &= \sum_{r=1}^R a_{m,r}^{(p)} - \sum_{\mathbf{i}_m^{(p)}} \left[\mathbf{x}_{\mathbf{i}_m^{(p)}}^{(p)} \log \left(\sum_{r=1}^R b_{\bar{\mathbf{i}}_m^{(p)}, r} a_{m,r}^{(p)} \right) \right]. \end{aligned}$$

In the first RHS term of equation (4.7), we have $\mathbf{e}^T \mathbf{B}^{(p)} \mathbf{a}_m^{(p)} = \sum_{r=1}^R a_{m,r}^{(p)}$ due to the simplex constraint on the rows of $\mathbf{B}^{(p)}$. Therefore, for each subproblem we only need to compute and store a $J_m^{(p)} \times R$ submatrix of $\mathbf{B}^{(p)}$ in which the $J_m^{(p)}$ columns correspond to nonzero elements in the vector $\mathbf{x}_m^{(p)}$, which can be calculated via

$$(4.8) \quad \mathbf{B}_{i_p}^{(p)} = \left(\circledast_{q \in \{1:P\} \setminus p} \mathbf{\Phi}^{(q)}[\mathbf{i}_{q,m}^{(p)}, :] \right) \circledast \Psi[\mathbf{n}_m^{(p)}, :].$$

Similarly, minimizing $f_m(\mathbf{a}_m^{(p)})$ can also be viewed as finding the maximum likelihood solution of a Poisson linear regression problem with identity link, in which $\mathbf{B}_m^{(p)}$ is a $J_m^{(p)} \times R$ matrix, $\mathbf{x}_m^{(p)}$ is a $J_m^{(p)} \times 1$ count vector, $\mathbf{a}_m^{(p)}$ is the $R \times 1$ nonnegative regression coefficients.

The block nonlinear GS algorithm for maximum likelihood estimation of our Poisson CP-BTD model is summarized in Algorithm 1. The algorithm iterates between updating the tensor loading factor matrices and the factor usage; both steps boil down to a number of convex optimization subproblems. Additional regularizers can be added to promote special properties, such as sparsity or group-sparsity, but the resulting penalized maximum likelihood problem might not be convex. In Section 4.3 we propose a solver

Algorithm 1 Block nonlinear Gauss-Seidel algorithm for Poisson CP-BTD

Input: Multiresolution adjacency tensor \mathcal{X} , the number of terms H , the CP rank R_h ,
Initialize \mathcal{D}_h
repeat
 % Given motifs $\{\mathcal{D}_h : h = 1, \dots, H\}$, update factor usage Υ ;
 for $n = 1$ **to** N **do**
 Calculate $\mathbf{D}^{[n]}$ according to equation (4.5);
 $\mathbf{v}_n = \arg \min_{\mathbf{v}_n \geq 0} f_n(\mathbf{v}_n) \equiv \sum_{h=1}^H v_{h,n} - \sum_{j=1}^{J_n} x_{j,n} \log(\sum_{h=1}^H d_{j,h}^{[n]} v_{h,n})$;
 end for
 Set $\mathbf{S} = \Omega \Upsilon$, $\boldsymbol{\tau} = \mathbf{S} \mathbf{e}$, $\mathbf{T} = \text{diag}(\boldsymbol{\tau})$, $\boldsymbol{\Psi} = \mathbf{T}^{-1} \mathbf{S}^T$;
 for $p = 1$ **to** P **do**
 % Given Υ and $\mathbf{A}^{(q)}$, $q = 1, \dots, P$, $q \neq p$, update $\boldsymbol{\Phi}^{(p)}$;
 for $m = 1$ **to** I **do**
 Calculate $\mathbf{B}_m^{(p)}$ according to equation (4.8);
 $\mathbf{a}_m^{(p)} = \arg \min_{\mathbf{a}_m^{(p)} \geq 0} f_m(\mathbf{a}_m^{(p)}) \equiv \sum_{r=1}^R a_{r,m}^{(p)} - \sum_{j=1}^{J_m^{(p)}} x_{m,j}^{(p)} \log\left(\sum_{r=1}^R b_{j,r}^{(p)} a_{r,m}^{(p)}\right)$;
 end for
 Set $\boldsymbol{\rho} = \mathbf{A}^{(p)} \mathbf{e}$, update $\boldsymbol{\Phi}^{(p)} = \mathbf{A}^{(p)} [\text{diag}(\boldsymbol{\rho})]^{-1}$;
 Update $\omega_{r_h, h} = \rho_{r_h, h} / \sum_{r_h=1}^{R_h} \rho_{r_h, h}$, $\forall (r_h, h)$;
 end for
until Convergence criterion is satisfied on all subproblems
Output: Ω , $\{\boldsymbol{\Phi}^{(p)}\}_{p=1:P}$, Υ

for sparse Poisson regression problems based on a Minorize-Maximization (MM) algorithm [Hunter and Lange (2004)], which iteratively operates on local convex surrogates and reaches a local optimum.

4.2. *Poisson regression with identity link.* In our Poisson CP-BTD model, the subproblems arising from the nonlinear GS procedures in Section 4.1 take the form of minimizing the negative log-likelihood of a special form of Poisson linear regression problem with column stochasticity constraints on the covariate matrix. The choice of Poisson model has considerable computational benefits over the Gaussian. To see this, denoting the observations $\mathbf{x} \in \mathbb{Z}^{M \times 1}$, the covariate matrix $\mathbf{A} \in [0, 1]^{M \times R}$, $\|\mathbf{a}_r\|_1 = 1$, and the non-zero subset $\mathbf{x}_+ \in \mathbb{Z}_+^{J \times 1}$, the corresponding covariate submatrix $\mathbf{A}_+ \in [0, 1]^{J \times K}$, $\mathbf{b} \geq 0$ are the $K \times 1$ unknown nonnegative regression coefficients, the objective function is written as,

$$\begin{aligned}
 f(\mathbf{b}; \mathbf{x}, \mathbf{A}) &= \sum_{m=1}^M \sum_{k=1}^K a_{k,j} b_k - \sum_{m=1}^M x_m \log \left(\sum_{k=1}^K a_{k,m} b_k \right) \\
 (4.9) \quad &= \sum_{k=1}^K b_k - \sum_{j=1}^J x_j \log \left(\sum_{k=1}^K a_{k,j} b_k \right) = f(\mathbf{b}; \mathbf{x}_+, \mathbf{A}_+).
 \end{aligned}$$

Therefore, this objective function in equation (4.9) only depends on the positive observations and its corresponding predictors. This feature has also been utilized in Chi and Kolda (2012) and Hansen, Plantenga and Kolda (2015) in developing efficient CP-APR algorithms. As already elaborated in Section 4.1, the sparse implementation achieves significant memory and computation savings without loss of accuracy. As a result, the computation of our algorithm scales linearly with the number of unique edges observed.

Minimizing equation (4.9) is a convex problem. Here we adopt the MM solver [Chi and Kolda (2012)] with closed-form updates while other solvers based on Newton methods [Hansen, Plantenga and Kolda (2015)] are also applicable. Starting from \mathbf{b}_0 vector with all elements positive,

$$\begin{aligned}
 f(\mathbf{b}; \mathbf{x}, \mathbf{A}) &= \sum_{k=1}^K b_k - \sum_{j:x_j>0} x_j \log \left(\sum_{k=1}^K q_{k,j} \frac{b_k a_{k,j}}{q_{k,j}} \right) \\
 (4.10) \quad &\leq \sum_{k=1}^K b_k - \sum_{j:x_j>0} \sum_{k=1}^K x_j q_{k,j} \log \left(\frac{b_k a_{k,j}}{q_{k,j}} \right) = Q(\mathbf{b}|\mathbf{b}^{\text{old}}).
 \end{aligned}$$

In each iteration, setting the first order derivative $Q'(\mathbf{b}|\mathbf{b}^{\text{old}})$ to zero yields the closed-form updating equation

$$b_k = \sum_{j:x_j>0} q_{k,j} x_j, \quad q_{k,j} = \frac{b_k^{\text{old}} a_{k,j}}{\sum_{k=1}^K b_k^{\text{old}} a_{k,j}}.$$

4.3. *Automatic adaptation of model dimensions.* In practice, it remains a challenge to choose the model dimension parameters $\{R_h, H\}$. Intuitively, the rank of \mathcal{D}_h determines the complexity of the motifs; this should not be too high for interpretability. H shall be set to a large number to enable over-complete representation with greater flexibility. We set both $\{R_h, H\}$ to upper bound values and rely on adaptive group sparsity regularizers to automatically shrink the redundant dimensions to zero. The multivariate Poisson regression in equation (4.11) with group sparse regularizers replaces the univariate Poisson regression problems as the basic computation unit,

$$(4.11) \quad \min_{\mathbf{B} \in \mathbb{R}_+^{K \times N}} \sum_{n=1}^N f_n(\mathbf{b}_n; \mathbf{x}_n, \mathbf{A}_n) + \beta \sum_{k=1}^K g_k(\mathbf{b}_k),$$

where $f_n(\mathbf{b}_n; \mathbf{x}_n, \mathbf{A}_n) = \sum_{k=1}^K b_{k,n} - \sum_{j=1}^{J_n} x_j \log \left(\sum_{k=1}^K a_{k,j} b_{k,n} \right)$, and β is the regularization parameter. To incorporate the adaptive shrinkage mechanism, we impose group sparse regularizers on the rows of \mathbf{B} , which take the form of

a log-sum penalty [Candes, Wakin and Boyd (2008); Larsson and Ugander (2011); Armagan, Dunson and Lee (2013)] $g_k(\mathbf{b}_k) = \log(\sum_{n=1}^N b_{k,n} + \epsilon)$, $\epsilon > 0$. We solve this problem via MM. Using the supporting hyperplane property of convex functions (negative logarithm),

$$\begin{aligned} \sum_{k=1}^K g_k(\mathbf{b}_n) &= \sum_{k=1}^K \log\left(b_{k,n} + \sum_{-n} b_{k,n} + \epsilon\right) \leq \sum_{n=1}^N \sum_{k=1}^K \frac{b_{k,n}}{\epsilon + \sum_{n=1}^N b_{k,n}^{\text{old}}} + \text{const} \\ &:= \sum_{n=1}^N \tilde{g}_n(\mathbf{b}_n | \mathbf{B}^{\text{old}}), \end{aligned}$$

this corresponds to a reweighted ℓ_1 penalty. Given the old updates $\mathbf{B}_n^{\text{old}}$, the surrogate function still separates into N additive terms, and the objective function can be rewritten as

$$\min_{\mathbf{b}_n \in \mathbb{R}_+^{K \times 1}} \sum_{n=1}^N \left[f_n(\mathbf{b}_n; \mathbf{x}_n, \mathbf{A}_n) + \beta \tilde{g}_n(\mathbf{b}_n | \mathbf{B}^{\text{old}}) \right].$$

For the n th subproblem, similarly to equation (4.10), we initialize $\mathbf{b}_{n,0}$ with an all positive vector,

$$\begin{aligned} f_n + \tilde{g}_n &= \sum_{k=1}^K b_{k,n} - \sum_{j:x_j > 0} x_j \log\left(\sum_{k=1}^K q_{k,j} \frac{b_{k,n} a_{k,j}}{q_{k,j}}\right) + \beta \sum_{k=1}^K \frac{b_{k,n}}{\epsilon + \sum_{n=1}^N b_{k,n}^{\text{old}}}, \\ &\leq \sum_{k=1}^K b_{k,n} - \sum_{j:x_j > 0} \sum_{k=1}^K q_{k,j} x_j \log\left(\frac{b_{k,n} a_{k,j}}{q_{k,j}}\right) + \beta \sum_{k=1}^K \frac{b_{k,n}}{\epsilon + \sum_{n=1}^N b_{k,n}^{\text{old}}} \\ &:= Q_n(\mathbf{b} | \mathbf{B}^{\text{old}}). \end{aligned}$$

Setting the first order derivative $Q'_n(\mathbf{b} | \mathbf{B}^{\text{old}})$ to zero yields the closed-form updating equation,

$$b_{k,n} = w_{k,n} \sum_{j:x_j > 0} q_{k,j} x_j, \quad w_{k,n} = \frac{1}{1 + \beta \frac{1}{\epsilon + \sum_{n=1}^N b_{k,n}^{\text{old}}}}, \quad q_{k,j} = \frac{\tilde{b}_k a_{k,j}}{\sum_{k=1}^K \tilde{b}_k a_{k,j}}.$$

The adaptive shrinkage mechanism works as follows: if one row is important and $\sum_{n=1}^N b_{k,n}^{\text{old}}$ is large, $\beta/(\epsilon + \sum_{n=1}^N b_{k,n}^{\text{old}})$ will be small, the corresponding weight $w_{k,n} \approx 1$, and $b_{k,n}^{\text{mle}} = \sum_{j:x_j > 0} q_{k,j} x_j$ is kept untouched. On the contrary, if a certain row is redundant and $\sum_{n=1}^N b_{k,n}^{\text{old}}$ is small, $\beta/(\epsilon + \sum_{n=1}^N b_{k,n}^{\text{old}})$ will be very large and the corresponding weight $w_{k,n} \approx 0$, so $b_{k,n}^{\text{mle}}$ will be shrunk very aggressively toward 0.

We encourage group sparsity both in the columns of the tensor factor loading matrices $\mathbf{A}^{(p)}$ and in the rows of the factor score matrix Υ . The log-sum penalty terms used are as follows,

$$g(\mathbf{A}^{(p)}) = \sum_{r=1}^R g_r \left(\sum_{i_p=1}^{I_p} a_{r,i_p}^{(p)} \right) = \sum_{r=1}^R \log \left(\sum_{i_p=1}^{I_p} a_{r,i_p}^{(p)} + \epsilon \right),$$

$$g(\Upsilon) = \sum_{h=1}^H g_h \left(\sum_{n=1}^N v_{h,n} \right) = \sum_{h=1}^H \log \left(\sum_{n=1}^N v_{h,n} + \epsilon \right).$$

These adaptive shrinkage regularizers facilitate automatic adaptations of the number of effective motifs H and render each motif to have a different level of complexity, which is upper bounded by R_h (Figure 6 provides an illustration).

5. Application to FIFA 2014 World Cup Passing Networks. Our Poisson CP-BTD model can serve as an exploratory factor analysis tool for soccer passing networks (described in Section 1.1). The model parameters are estimated by the block nonlinear GS algorithm introduced in Section 4. The computation is performed on a laptop computer with 4 Intel Core i7 (2 GHz) and 16 GB of RAM. Setting the maximum number of outer loops of the block nonlinear GS algorithm to be 100 and the maximum number of inner-loop iterations in solving the Poisson regression subproblems to be 250, our MATLAB implementation takes about 1.8 hours to run. The implementation is built upon Tensor Toolbox Version 2.6 [Bader et al. (2015)]. The code for the proposed algorithm will be available on Github.

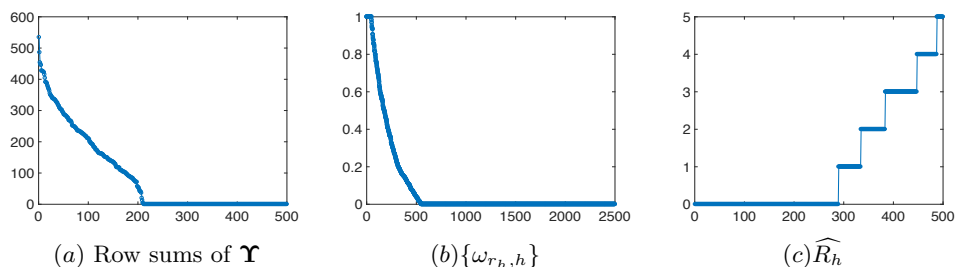


FIG 6. Automatic adaption of model dimensions via log-sum group shrinkage

The model complexity is controlled by both the model dimensional parameters (H, R_h) and the strength of group shrinkage. To ensure the model has large capacity and easy-to-interpret representations, we set $H = 500$, $R_h = 5$ with regularization parameters $\beta = 0.001 \times J$, where J is the number

of effective predictors in Equation (4.9). Figure 6(a) shows the row sums of the factor usage matrix Υ sorted in descending order, in which 211 of the 500 values depart from zero. Figure 6(b) plots the excitation weights of the individual rank-one components sorted in descending order. The “nonnegative-rank” of \mathcal{D}_h can therefore be determined via $\widehat{R}_h = \sum_{r_h} \mathbb{1}(\omega_{r_h, h} > 10^{-10})$. Figure 6(c) shows a variety of “nonnegative-rank” numbers of each motifs \mathcal{D}_h , ranging from 0 to 5. The adaptive group sparsity regularizer introduced in Section 4.3 provides the practitioner an additional tolerance in balancing between parsimony (the model shall have fewer factors with simpler interpretation) and plausibility (that there are enough factors to adequately account for intricate structures in the data).

Penalized maximum likelihood estimation of our Poisson CP-BTD model reduces the multiresolution adjacency tensor \mathcal{X} into a $H \times N$ factor score matrix $\widehat{\Upsilon}$, mapping from the ambient dimension of observed passing networks to a lower dimensional intrinsic space. Letting $\boldsymbol{\eta} = \mathbf{e}\widehat{\Upsilon}$, $\mathbf{R} = \text{diag}(\boldsymbol{\eta})$, we have $\boldsymbol{\Theta} = \widehat{\Upsilon}\mathbf{R}^{-1}$ with each column satisfying the condition $\widehat{\theta}_{h,n} \geq 0$, $\sum_{h=1}^H \widehat{\theta}_{h,n} = 1$. The Poisson intensity parameter $\eta_n > 0$ indicates the rate of a team conducting completed passes in a particular game, and $\widehat{\boldsymbol{\theta}}_n$ represent the admixture proportion of subnetwork h in replicate n . While the variations of both parameters across replicates could have non-negligible effects on driving the team performance and determining the competition outcomes, we decouple these two different kinds of variations and focus on the later, as we are particularly interested in understanding what kind of subnetwork patterns contribute to the outcome.

We measure the team performance using external predictor variables $\mathbf{y}_n = \{w_n, l_n\}$, where w_n is the number of goals scored and l_n is the number of goals lost, accounting for the overall quality of the team’s offense and defense. Other relevant metrics such as the ball possession time, the number of shots created, and the number of hits in the attacking third can be included as well according to user’s interest. To find the lower dimensional embedding underlying the passing networks that is predictive of the outcome variables, we apply the multinomial inverse regression (MNIR) approach [Taddy (2013)] to the factor usage space as a post-processing step. According to the Fisher Neyman factorization theorem, the sufficient reduction (SR) score for $\boldsymbol{\theta}_n$ is defined via $\mathbf{z}_n = \boldsymbol{\Gamma}^T \boldsymbol{\theta}_n$, where $\theta_{h,n} = \exp[\mu_{h,n}] / \sum_{h'=1}^H \exp[\mu_{h',n}]$ and $\mu_{h,n} = \alpha_h + \gamma_{1,h}w_n + \gamma_{2,h}l_n$, $\boldsymbol{\Gamma} \in \mathbb{R}^{H \times 2}$, α_h is the intercept. The combination of our model and the MNIR approach provides results that are interpretable in terms of showing specific motifs in the passing network that contribute to prediction. The passing network objects are converted into a set of coordinates, which can aid team comparison. We use R package **textir** for the

estimation of MNIR parameters with ℓ_1 regularization.

Traditionally, the teams’ offensive or defensive performance in a game can be quantified via the number of goals scored or lost, therefore the gap between the two opponents is often measured by the goal difference. Table 2 and Table 3 listed 10 games with the highest goal difference and 10 games with the lowest goal difference at the 2014 World Cup. There are many ties and team performance evaluation or comparison based solely on box scores is quite limited both within and across games. For example, Iran 0:0 Nigeria in Game #12: does this mean the defensive qualities of both teams are equally good, or maybe the offensive abilities of both teams are equally bad? Germany 4:0 Portugal in Game #13 and Croatia 4:0 Cameroon in Game #18: their scores are exactly the same but which win comes relatively easier? John Anthony Brooks scored with just 4 minutes left to play as the USA finally defeated Ghana 2:1 in Game #14, is this a well-deserved victory?

TABLE 2
Top 10 games with the highest goal difference

Game	Competition Outcome
61	Germany 7:1 Brazil
3	Netherlands 5:1 Spain
13	Germany 4:0 Portugal
18	Croatia 4:0 Cameroon
5	Colombia 3:0 Greece
10	France 3:0 Honduras
25	France 5:2 Switzerland
33	Brazil 4:1 Cameroon
35	Spain 3:0 Australia
41	Switzerland 3:0 Honduras

TABLE 3
Top 10 games with the lowest goal difference

Game	Competition Outcome
12	Iran 0:0 Nigeria
17	Brazil 0:0 Mexico
22	Greece 0:0 Japan
40	Costa Rica 0:0 England
42	Ecuador 0:0 France
59	Costa Rica 0:0 Netherlands
62	Argentina 0:0 Netherlands
16	Russia 1:1 South Korea
48	Algeria 1:1 Russia
49	Brazil 1:1 Chile

Figure 7 shows the 2- dimensional embedding of the 128 passing networks. The x-coordinate and y-coordinate refer to $\gamma_1^T \theta_n$ and $-\gamma_2^T \theta_n$ respectively. Higher values in the SR scores indicate higher offense (or defense) abilities. The color denotes the match outcome (win, draw, or loss). For the sake of clarity, only the names of a subset of the networks are displayed (see Appendix B for figures with all networks’ names displayed). The 2- dimensional embedding space of passing networks is discriminative with respect to the competition outcomes. In general, teams located in the first orthant are those who proficient in both offense and defense and win the competitions. On the contrary, teams located in the third orthant are those who are weak in both offense and defense, and are also those tending to lose the games.

Supervised dimension reduction on the tensor factor scores merges information from both passing networks and match outcomes. From Figure 7,

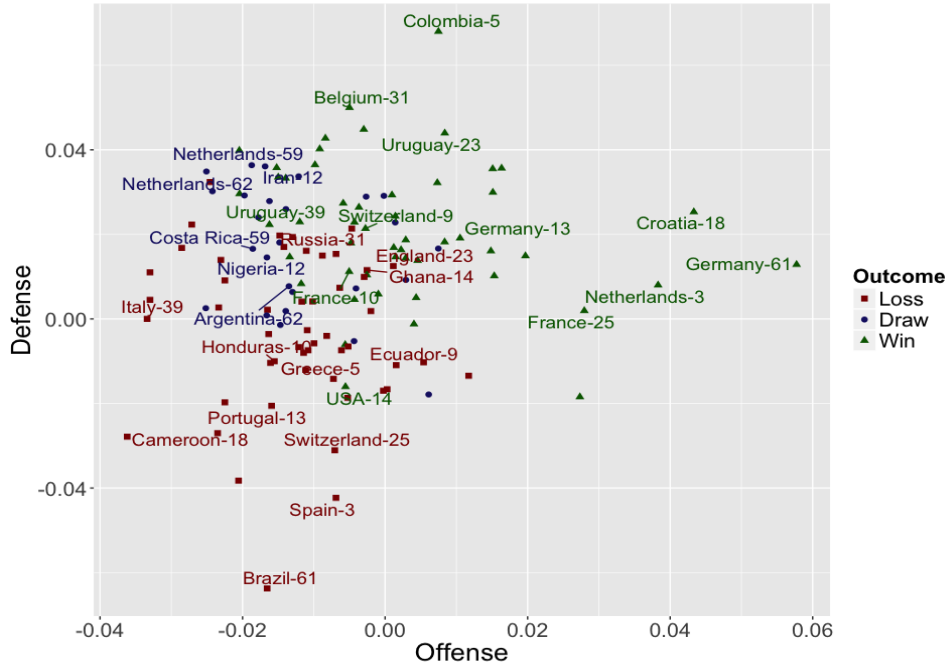


FIG 7. *Supervised dimension reduction of soccer passing networks*

we can see that teams' offense and defense performances vary against different opponents in different stage of the tournament. The Netherlands team was offensively very aggressive in their opener against Spain (Game #3), but played more conservatively with high defensive quality in their quarter-finals against Costa Rica (Game #59) and semi-finals against Argentina (Game #62). The Iran team demonstrated a high quality of defense in Game #12, which is comparable to Netherlands-59 and Netherlands-62, and better than their opponent —Nigeria in that game. The reason for not winning the game is probably due to their poor offense. According to the distance between coordinates of the team-opponent pairs projected on the identity line in Figure 7, Croatia 4:0 Cameroon is more a one-sided game than Germany 4:0 Portugal. Interestingly, in the Game #14 Ghana 1:2 USA, our results suggest that Ghana had better offense and defense. This finding also seems consistent with other match statistics comparisons between the two teams, including shots/shots on goal 21/8 – 8/7, corner kicks 7 – 3, and ball possession 59% – 41%. The victory of the USA is attribute to other factors that the data did not capture.

We further identify some key passing patterns that play a role in driv-

ing team performance. The values of the regression coefficients γ_1 and $-\gamma_2$ manifest the effectiveness of passing network motifs in creating goals and avoiding loss goals. Under the sparse regularization, most of the network motifs are pruned out, so they are uncorrelated with the match outcomes. We rank the effectiveness of passing motifs in term of offense and defense according to the value of the regression coefficients γ_1 and $-\gamma_2$. Some examples of offensively effective, offensively ineffective, defensively effective, and defensively ineffective motifs are shown in Figure 12, Figure 13, Figure 14, and Figure 15, respectively. Comparing against other approaches based on network statistics, these multiresolution network motifs provide the domain experts (professional coaches, soccer analysts) with results that are visually comprehensive, and allow them better understanding of the repeated passing subnetworks emerging from the 2014 World Cup, while (more importantly) identifying the patterns that most contribute to the outcome.

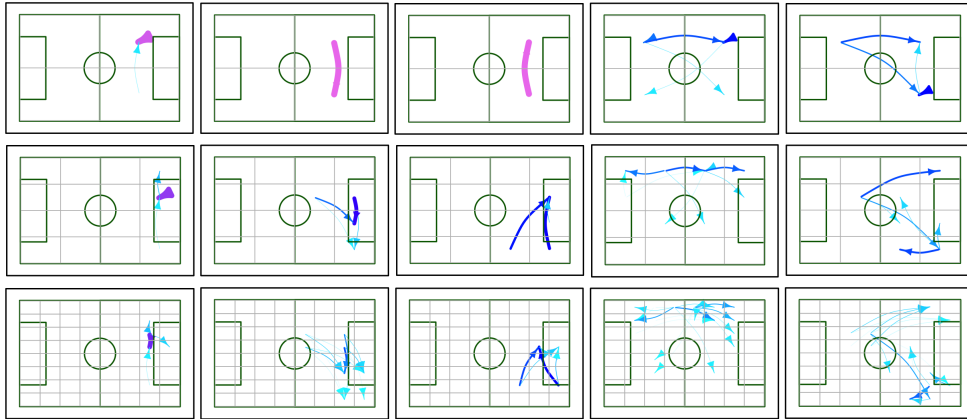


FIG 8. *Offensively effective motifs (first row $S = 1$, second row $S = 2$, third row $S = 3$)*

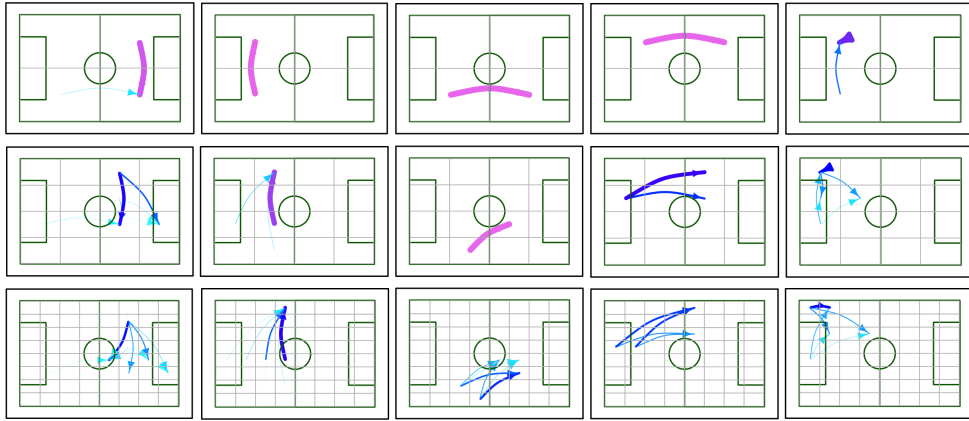


FIG 9. *Offensively ineffective motifs* (first row $S = 1$, second row $S = 2$, third row $S = 3$)

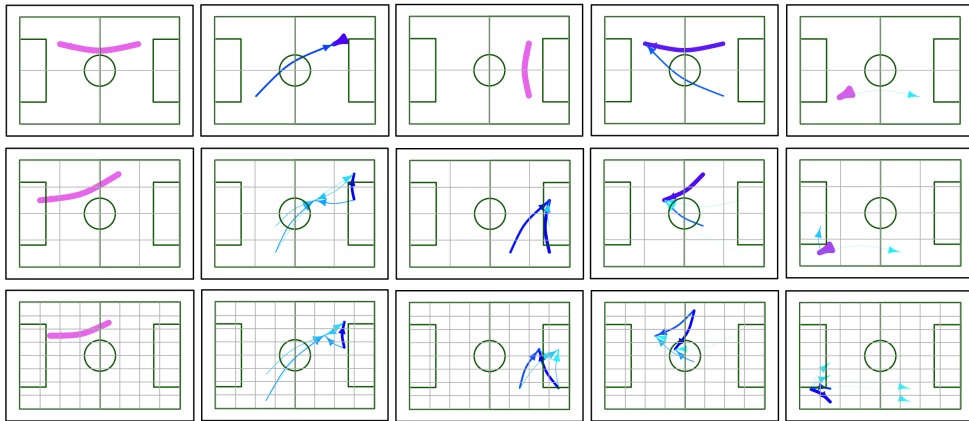


FIG 10. *Defensively effective motifs* (first row $S = 1$, second row $S = 2$, third row $S = 3$)

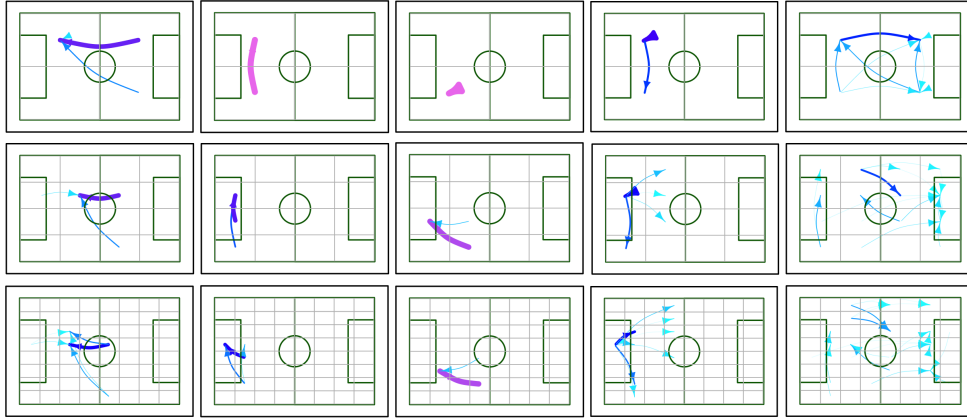


FIG 11. *Defensively ineffective motifs* (first row $S = 1$, second row $S = 2$, third row $S = 3$)

6. Conclusion. We have presented a multiresolution adjacency tensor representation for replicated, directional networks with spatial registrations. Based on the higher-order tensorization scheme, a novel Poisson nonnegative tensor factor model is proposed, which borrows information across scales and produces coherent coarse-to-fine low-rank subnetworks with natural interpretations. We also developed a convergent, computationally and memory efficient optimization algorithm, which is potentially parallelizable. The adaptive shrinkage mechanism balances between flexibility and parsimony in overcomplete representation learning.

Motivated by relational event data arising in sports analytics, the proposed model is also applicable to many other types of data that contain a replicated spatial network structure. The proposed algorithm offers computational promise in handling massive and fine-grained spatial networks, such as brain connectome networks, traffic flow networks, etc.

To investigate how the passing patterns drive the competition outcomes, we extend our exploratory factor analysis tool to the supervised case by allowing the admixture proportions to depend on the predictor variables in a separate postprocessing step. It is also appealing to jointly model the passing networks with outcomes and develop a supervised dimensionality reduction directly on the network-variate data in an optimal manner for predicting outcomes. It is additionally worth noticing that the passing network is also dependent on the defense being faced; our current approach does not consider the offense-defense interaction between pairs of passing networks.

APPENDIX A: EM ALGORITHM FOR MAXIMIZING THE
LIKELIHOOD OF POISSON CP-BTD MODEL

The EM algorithm maximizes the Poisson likelihood with respect to the parameters $\Theta = \{\Upsilon, \Phi, \Omega\}$. The expectation of the complete-data log likelihood denoted as $Q(\Theta|\Theta^{\text{old}})$ is given by,

$$Q(\Theta|\Theta^{\text{old}}) = \sum_{i_{1:P}} \sum_{n=1}^N \left(\sum_{h=1}^H \sum_{r=1}^{R_h} Q_{j,t}(\Theta|\Theta^{\text{old}}) \right) = \sum_j \sum_t Q_{j,t}(\Theta|\Theta^{\text{old}}),$$

and

$$Q_{j,t}(\Theta|\Theta^{\text{old}}) = - \int_{z_{j,t}} \left[\log p(z_{j,t}|\Theta) \right] p(z_{j,t}|\Theta^{\text{old}}, x_j) dz_{j,t},$$

where

$$\log p(z_{j,t}|\Theta) = -\lambda_{j,t} + z_{j,t} \log \left(\lambda_{j,t} \right), \quad j = (i_1, \dots, i_6, n), \quad t = (r_h, h),$$

$$p(z_{j,t}|\Theta^{\text{old}}, x_j) = \text{Binomial}(z_{j,t}; x_j, p_{j,t}^{\text{old}}), \quad p_{j,t}^{\text{old}} = \frac{\tilde{\lambda}_{j,t}}{\sum_{t=1}^T \tilde{\lambda}_{j,t}}.$$

So in the E step,

$$Q_{j,t}(\Theta|\Theta^{\text{old}}) = \lambda_{j,t} - \langle z_{j,t} \rangle \log \left(\lambda_{j,t} \right), \quad \langle z_{j,t} \rangle = x_j p_{j,t}^{\text{old}} = \frac{x_j \tilde{\lambda}_{j,t}}{\sum_{t=1}^T \tilde{\lambda}_{j,t}},$$

and in the M step,

1. Update $v_{h,n}$

$$\max_{v_{h,n} > 0} \sum_{j=1}^J \sum_{t=1}^T \left[\omega_{r_h, h} v_{h,n} \prod_{p=1}^P \phi_{i_p, r_h, h}^{(p)} - \langle z_{j,t} \rangle \log(v_{h,n}) \right],$$

$$\left[\sum_{i_{1:P}, r} \omega_{r_h, h} \prod_{p=1}^P \phi_{i_p, r_h, h}^{(p)} - \sum_{i_{1:P}, r} \langle z_{j,t} \rangle \frac{1}{v_{h,n}} \right] = 0,$$

$$v_{h,n} = \frac{\sum_{i_{1:P}, r} \langle z_{j,t} \rangle}{\sum_{i_{1:P}} \sum_{r=1}^{R_h} \omega_{r_h, h} \prod_{p=1}^P \phi_{i_p, r_h, h}^{(p)}} = \sum_{i_{1:P}, r, h} \langle z_{j,t} \rangle.$$

2. Update $a_{i_p, r_h, h}^{(p)}$, $p = 1, \dots, P$

$$\begin{aligned} & \max_{\phi_{r_h, h} \in \mathbb{S}^{U-1}} \sum_{j=1}^J \sum_{t=1}^T \left[\omega_{r_h, h} \nu_{h, n} \prod_{p=1}^P \phi_{i_p, r_h, h}^{(p)} - \langle z_{j, t} \rangle \log(\phi_{i_p, r_h, h}^{(p)}) \right] \\ & + \alpha_{r_h, h}^{(p)} \left(\sum_{i_p=1}^{I_p} \phi_{i_p, r_h, h}^{(p)} - 1 \right), \end{aligned}$$

$$\sum_{\mathbf{i}_{\{1:p\} \setminus p, n, h}} \omega_{r_h, h} \nu_{h, n} \prod_{\{1:p\} \setminus p} \phi_{i_p, r_h, h}^{(p)} - \sum_{\mathbf{i}_{\{1:p\} \setminus p, n, h}} \langle z_{j, t} \rangle \frac{1}{\phi_{i_p, r_h, h}^{(p)}} + \alpha_{r_h, h}^{(p)} = 0,$$

$$\phi_{i_p, r_h, h}^{(p)} = \frac{\sum_{\mathbf{i}_{\{1:p\} \setminus p, n, h}} \langle z_{j, t} \rangle}{\sum_{i_p=1}^{I_p} \sum_{\mathbf{i}_{\{1:p\} \setminus p, n, h}} \langle z_{j, t} \rangle}.$$

3. Update ω_h ,

$$\begin{aligned} & \max_{\omega_h \in \mathbb{S}^{R_h-1}} \sum_{j=1}^J \sum_{t=1}^T \left[\omega_{r_h, h} \nu_{h, n} \prod_{p=1}^P \phi_{i_p, r_h, h}^{(p)} - \langle z_{j, t} \rangle \log(\omega_{r_h, h}) \right] \\ & + \gamma_h \left(\sum_{r_h=1}^{R_h} \omega_{r_h, h} - 1 \right), \end{aligned}$$

$$\omega_{r_h, h} = \frac{\sum_j \langle z_{j, t} \rangle}{\sum_{r=1}^{R_h} \sum_j \langle z_{j, t} \rangle}.$$

APPENDIX B: SUPERVISED PASSING NETWORK EMBEDDING RESULTS

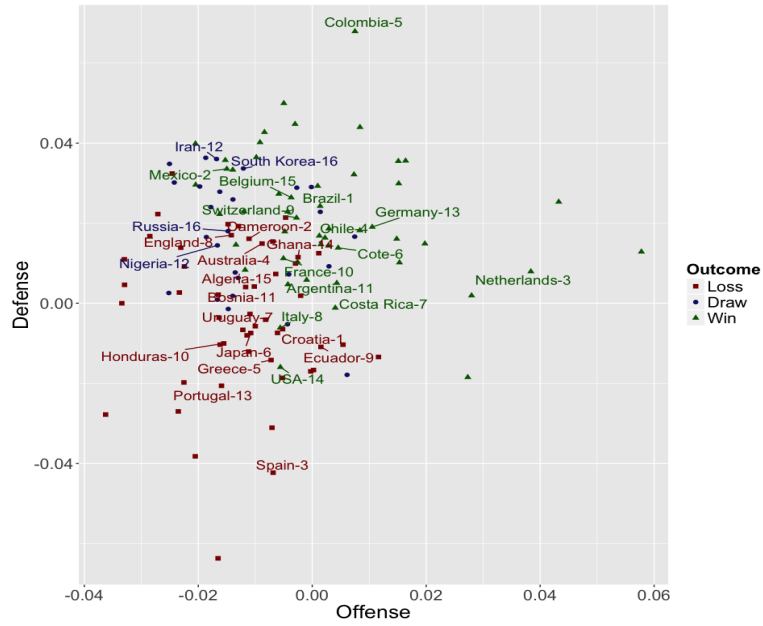


FIG 12. *Supervised embedding of passing networks (Game #1 – 16)*

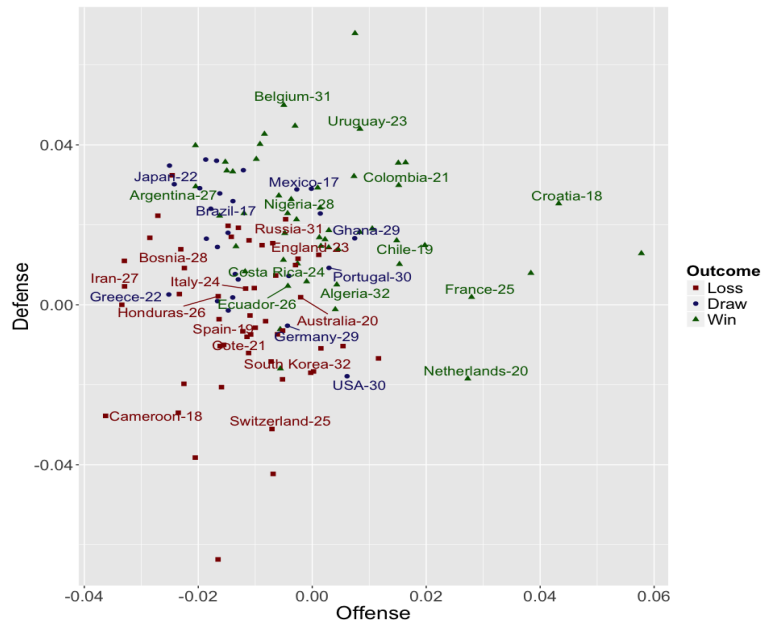


FIG 13. *Supervised embedding of networks (Game #17 – 32)*

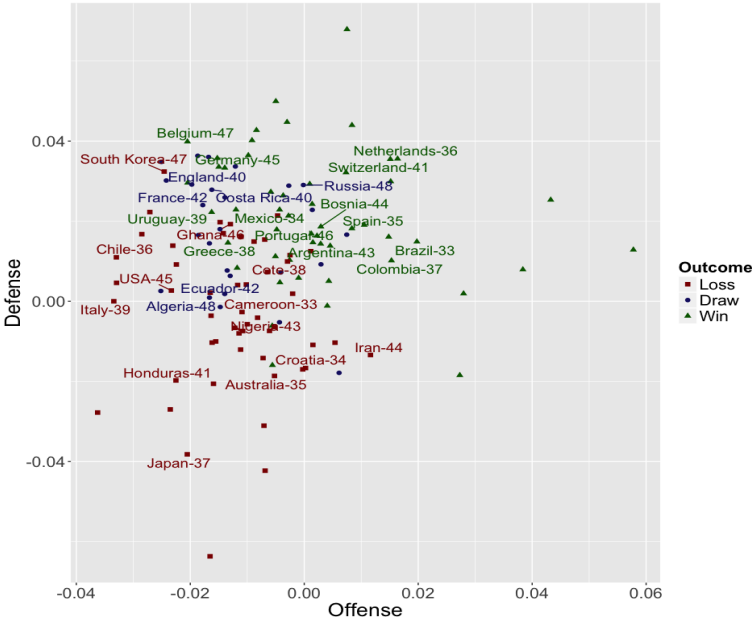


FIG 14. Supervised embedding of networks (Game #33 – 48)

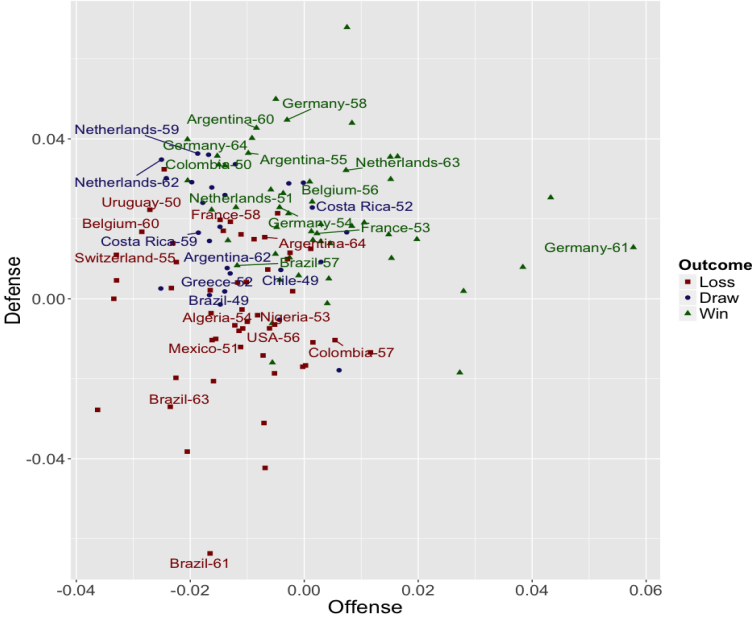


FIG 15. Supervised embedding of networks (Game #49 – 64)

ACKNOWLEDGEMENTS

This work was supported by the grant W911NF-16-1-0544 of the U.S. Army Research Institute for the Behavioral and Social Sciences (ARI).

REFERENCES

- AHN, Y.-Y., BAGROW, J. P. and LEHMANN, S. (2010). Link communities reveal multiscale complexity in networks. *Nature* **466** 761.
- AIROLDI, E. M., BLEI, D. M., FIENBERG, S. E. and XING, E. P. (2008). Mixed membership stochastic blockmodels. *Journal of Machine Learning Research* **9** 1981–2014.
- ARMAGAN, A., DUNSON, D. B. and LEE, J. (2013). Generalized double Pareto shrinkage. *Statistica Sinica* **23** 119.
- BADDELEY, A., BÁRÁNY, I. and SCHNEIDER, R. (2007). Spatial point processes and their applications. *Lecture Notes in Mathematics-Springer-Verlag* **1892**.
- BADER, B. W., KOLDA, T. G. et al. (2015). MATLAB Tensor Toolbox Version 2.6. Available online.
- BALL, B., KARRER, B. and NEWMAN, M. E. (2011). Efficient and principled method for detecting communities in networks. *Physical Review E* **84** 036103.
- BARTHÉLEMY, M. (2011). Spatial networks. *Physics Reports* **499** 1–101.
- BRAY, J. R. and CURTIS, J. T. (1957). An ordination of the upland forest communities of southern Wisconsin. *Ecological Monographs* **27** 325–349.
- CANDES, E. J., WAKIN, M. B. and BOYD, S. P. (2008). Enhancing sparsity by reweighted ℓ_1 minimization. *Journal of Fourier Analysis and Applications* **14** 877–905.
- CARON, F. and FOX, E. B. (2017). Sparse graphs using exchangeable random measures. *Journal of the Royal Statistical Society: Series B (Statistical Methodology)* **79** 1295–1366.
- CERVONE, D., D’AMOUR, A., BORNN, L. and GOLDSBERRY, K. (2016). A multiresolution stochastic process model for predicting basketball possession outcomes. *Journal of the American Statistical Association* **111** 585–599.
- CHI, E. C. and KOLDA, T. G. (2012). On tensors, sparsity, and nonnegative factorizations. *SIAM Journal on Matrix Analysis and Applications* **33** 1272–1299.
- CICHOCKI, A., MANDIC, D., DE LATHAUWER, L., ZHOU, G., ZHAO, Q., CAIAFA, C. and PHAN, H. A. (2015). Tensor decompositions for signal processing applications: From two-way to multiway component analysis. *IEEE Signal Processing Magazine* **32** 145–163.
- CINTIA, P., RINZIVILLO, S. and PAPPALARDO, L. (2015). A network-based approach to evaluate the performance of football teams. In *Machine Learning and Data Mining for Sports Analytics Workshop, Porto, Portugal*.
- COHEN, J. E. and ROTHBLUM, U. G. (1993). Nonnegative ranks, decompositions, and factorizations of nonnegative matrices. *Linear Algebra and its Applications* **190** 149–168.
- DE LATHAUWER, L. (2008). Decompositions of a higher-order tensor in block terms—Part II: Definitions and uniqueness. *SIAM Journal on Matrix Analysis and Applications* **30** 1033–1066.
- DE LATHAUWER, L. and NION, D. (2008). Decompositions of a higher-order tensor in block terms—Part III: Alternating least squares algorithms. *SIAM Journal on Matrix Analysis and Applications* **30** 1067–1083.
- DUCH, J., WAITZMAN, J. S. and AMARAL, L. A. N. (2010). Quantifying the performance of individual players in a team activity. *PloS One* **5** e10937.

- DURANTE, D., DUNSON, D. B. et al. (2017). Bayesian inference and testing of group differences in brain networks. *Bayesian Analysis*.
- DURANTE, D., DUNSON, D. B. and VOGELSTEIN, J. T. (2017). Nonparametric Bayes modeling of populations of networks. *Journal of the American Statistical Association* 1–15.
- FRANKS, A., MILLER, A., BORNN, L. and GOLDSBERRY, K. (2015). Characterizing the spatial structure of defensive skill in professional basketball. *Annals of Applied Statistics* **9** 94–121.
- GOLDENBERG, A., ZHENG, A. X., FIENBERG, S. E., AIROLDI, E. M. et al. (2010). A survey of statistical network models. *Foundations and Trends® in Machine Learning* **2** 129–233.
- GRIPPO, L. and SCIANDRONE, M. (2000). On the convergence of the block nonlinear Gauss–Seidel method under convex constraints. *Operations Research Letters* **26** 127–136.
- HANSEN, S., PLANTENGA, T. and KOLDA, T. G. (2015). Newton-based optimization for Kullback–Leibler nonnegative tensor factorizations. *Optimization Methods and Software* **30** 1002–1029.
- HOFF, P. (2008). Modeling homophily and stochastic equivalence in symmetric relational data. In *Advances in Neural Information Processing Systems* 657–664.
- HOLLAND, P. W., LASKEY, K. B. and LEINHARDT, S. (1983). Stochastic blockmodels: First steps. *Social Networks* **5** 109–137.
- HUNTER, D. R. and LANGE, K. (2004). A tutorial on MM algorithms. *The American Statistician* **58** 30–37.
- KHOROMSKIJ, B. N. (2011). $O(d \log n)$ -quantics approximation of n^d tensors in high-dimensional numerical modeling. *Constructive Approximation* **34** 257–280.
- KIM, J., HE, Y. and PARK, H. (2014). Algorithms for nonnegative matrix and tensor factorizations: A unified view based on block coordinate descent framework. *Journal of Global Optimization* **58** 285–319.
- KOLACZYK, E. D. (1999). Bayesian multiscale models for Poisson processes. *Journal of the American Statistical Association* **94** 920–933.
- KOLDA, T. G. and BADER, B. W. (2009). Tensor decompositions and applications. *SIAM Review* **51** 455–500.
- LARSSON, M. O. and UGANDER, J. (2011). A concave regularization technique for sparse mixture models. In *Advances in Neural Information Processing Systems* 1890–1898.
- LEE, D. D. and SEUNG, H. S. (1999). Learning the parts of objects by non-negative matrix factorization. *Nature* **401** 788.
- LEWICKI, M. S. and SEJNOWSKI, T. J. (2000). Learning overcomplete representations. *Neural Computation* **12** 337–365.
- MILLER, A., BORNN, L., ADAMS, R. and GOLDSBERRY, K. (2014). Factorized point process intensities: A spatial analysis of professional basketball. In *International Conference on Machine Learning* 235–243.
- MØLLER, J. and WAAGEPETERSEN, R. P. (2007). Modern statistics for spatial point processes. *Scandinavian Journal of Statistics* **34** 643–684.
- NOWICKI, K. and SNIJDERS, T. A. B. (2001). Estimation and prediction for stochastic blockstructures. *Journal of the American Statistical Association* **96** 1077–1087.
- ORBANZ, P. and ROY, D. M. (2015). Bayesian models of graphs, arrays and other exchangeable random structures. *IEEE Transactions on Pattern Analysis and Machine Intelligence* **37** 437–461.
- OSELEDETS, I. V. (2010). Approximation of $2^d \times 2^d$ matrices using tensor decomposition. *SIAM Journal on Matrix Analysis and Applications* **31** 2130–2145.

- PEÑA, J. and TOUCHETTE, H. (2012). A network theory analysis of football strategies. In *Sports Physics: Proc. 2012 Euromech Physics of Sports Conference* 517–528.
- SCHMIDT, M. N. and MORUP, M. (2013). Nonparametric Bayesian modeling of complex networks: An introduction. *IEEE Signal Processing Magazine* **30** 110–128.
- SHASHUA, A. and HAZAN, T. (2005). Non-negative tensor factorization with applications to statistics and computer vision. In *Proceedings of the 22nd International Conference on Machine Learning* 792–799. ACM.
- TADDY, M. (2013). Multinomial inverse regression for text analysis. *Journal of the American Statistical Association* **108** 755–770.
- WANG, L., DURANTE, D., JUNG, R. E. and DUNSON, D. B. (2017). Bayesian network–response regression. *Bioinformatics* **33** 1859–1866.
- WILLSKY, A. S. (2002). Multiresolution Markov models for signal and image processing. *Proceedings of the IEEE* **90** 1396–1458.
- ZHOU, M. (2015). Infinite edge partition models for overlapping community detection and link prediction. In *Artificial Intelligence and Statistics* 1135–1143.
- ZHOU, J., BHATTACHARYA, A., HERRING, A. H. and DUNSON, D. B. (2015). Bayesian factorizations of big sparse tensors. *Journal of the American Statistical Association* **110** 1562–1576.